# Robust Estimation of HDR in fMRI using H Filters

Ratnarajah, T. (2010). Robust Estimation of HDR in fMRI using H Filters. IEEE TRANSACTIONS ON BIOMEDICAL ENGINEERING, 57(5), 1133-1142. [5415629]. DOI: 10.1109/TBME.2009.2039569

**Published in:**
IEEE TRANSACTIONS ON BIOMEDICAL ENGINEERING

# Robust Estimation of HDR in fMRI using $H^\infty$ Filters

S. Puthusserypady*, *Senior Member, IEEE*, Rui Jue, and T. Ratnarajah, *Senior Member, IEEE*

***Abstract*—Estimation and detection of the hemodynamic response (HDR) are of great importance in functional MRI (fMRI) data analysis. In this paper, we propose the use of three $H^\infty$ adaptive filters (*finite memory*, *exponentially weighted,* and *time-varying*) for accurate estimation and detection of the HDR. The $H^\infty$ approach is used because it safeguards against the worst case disturbances and makes no assumptions on the (statistical) nature of the signals [B. Hassibi and T. Kailath, in *Proc. ICASSP*, 1995, vol. 2, pp. 949–952; T. Ratnarajah and S. Puthusserypady, in *Proc. 8th IEEE Workshop DSP*, 1998, pp. 1483–1487]. Performances of the proposed techniques are compared to the conventional $t$-test method as well as the well-known LMSs and recursive least squares algorithms. Extensive numerical simulations show that the proposed methods result in better HDR estimations and activation detections.**

***Index Terms*—Activation detection, functional MRI (fMRI), hemodynamic response (HDR), $H^\infty$ filters.**

## I. Introduction

FUNCTIONAL MRI (fMRI) is a widely used noninvasive neuroimaging technique to investigate the changes in brain functions [3], [4]. It detects the blood-oxygen-level-dependent (BOLD) responses due to different brain activities [5]. The hemodynamic response (HDR) reflects the temporal properties of the human brain activities and its estimation is of great importance in the study of the brain functions [6]. fMRI experiments use two schemes of experiment designs, namely the block design and the event-related design [7]. Block designs are generally used in HDR detection because of its larger SNR. However, due to the temporal integration of the response signals in block design, the event-related design is preferred in investigating the temporal characteristics of the HDR [8].

The HDR is usually estimated through selective averaging procedures, in which many stimuli are presented and the responses averaged are time-locked to the stimuli [9]. This method does not take into account the overlap of responses and thus assumes that the interstimulus intervals (ISIs) are large enough such that consecutive HDRs do not overlap. Other well-known approaches used in HDR estimation include the use of time-series methods based on generalized linear models (GLMs) [10], [11]. The temporally overlapping responses were also modeled based on multiple regression within the GLM [12].

Studies in cerebral response have suggested that changes in intensity or duration have near-linear and additive effects on the BOLD response [13]. Also in [9], it is found that the fMRI BOLD signals summated in a roughly linear fashion across successive trials, even at short ISI (2–4 s). Studies have also shown that for large ISI (>4–6 s), the system consisting of the human brain and MRI scanner can be considered as a linear time-invariant (LTI) system [14]. While nonlinearities were observed in some cases (leading to the proposal of the Balloon model and the Volterra series model [15], [16]), the linearity assumption is found to hold in a wide range of experiments. This validates the means of estimating the HDR using the LTI approach, which assumes the linear summation of responses to each stimulus.

Parametric filter models, such as the Poisson filter and the Gamma filter, impose a specific shape on the linear filter coefficients and have been used in the LTI approach [17]. These parametric models may introduce some bias on the HDR function, since it is unlikely that they capture the shape variations of the HDR within the brain [18]. The method of estimating the HDR using an FIR filter was first performed in [19]. Though it is parametric in the sense that it fits a number of parameters, it does not impose a certain shape on the filter coefficients. Thus, the FIR filter method is known as the semiparametric approach and is more flexible than the Poisson and Gamma filters in reliably modeling the initial dip and the undershoot of the HDR [17]. Using the FIR filter model, HDR estimation can be simplified to be a deconvolution problem as follows:

$$\text{BOLD} = \text{input} \otimes \text{HDR} \tag{1}$$

where $\otimes$ denotes the convolution operation.

In system modeling, assumptions are often made on the statistical distributions of the noise. However, given the many causes of noise in fMRI signals, such as swallowing, head motion, as well as noise originating from the MRI scanner [20], we have insufficient information to conclude on the noise properties. The $H^\infty$ approach is introduced in robust control theory based on the hypothesis that the resulting *minmax* estimation techniques would be more robust and less sensitive to model uncertainties and parameter variations than the conventional techniques [21]. The use of $H^\infty$ algorithms in situations, where we have lack of statistical information with respect to noise, replaces the conventional methods of modeling the disturbance signal as a random process with a given spectral density, which rely heavily on the validity of the model assumptions and are hence limited in applications [2], [21].

Manuscript received May 25, 2009; revised October 8, 2009. First published February 17, 2010; current version published April 21, 2010. This work was supported by the Strategic Alliances and Partnerships strand of the Prime Ministers Initiative for International Education 2 (PMI2) under Grant RC 73 between Queens University Belfast and National University of Singapore. *Asterisk indicates corresponding author.*

*S. Puthusserypady is with the Department of Electrical Engineering, Technical University of Denmark, Kgs. Lyngby, Denmark (e-mail: spu@elektro.dtu.dk).

R. Jue is with the Department of Electrical and Computer Engineering, National University of Singapore, Singapore 117576, Singapore, and also with the DSO National Laboratories, Singapore 118230, Singapore (e-mail: rui_jue11@hotmail.com).

T. Ratnarajah is with the Institute for Electronics, Communications, and Information Technologies, Queen's University of Belfast, Belfast, BT3 9DT, United Kingdom (e-mail: t.ratnarajah@ieee.org).

Color version of one or more of the figures in this paper are available online at http://ieeexplore.ieee.org.

Digital Object Identifier 10.1109/TBME.2009.2039569

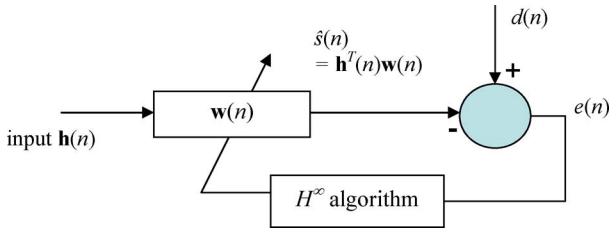


Fig. 1. Filter model.

In this paper, three $H^\infty$ adaptive algorithms, namely, the $H^\infty$ time-varying (TV), $H^\infty$ exponentially weighted (EW), and the $H^\infty$ finite-memory (FM) algorithms, are proposed for the estimation of HDR in fMRI. These algorithms cope with time variations in the HDR and are therefore suitable for fMRI data analysis. Through extensive numerical simulations, it is shown that these algorithms work well for the accurate estimation of HDR, and hence, the improved detection of activated areas of the brain.

## II. Method

From an engineering perspective, the HDR estimation can be regarded as a system modeling problem. The measured fMRI signal $d(n)$ at any particular voxel can be represented as follows [8]:

$$d(n) = h(n) \otimes w(n) + v(n) \tag{2}$$

$$= s(n) + v(n) \tag{3}$$

where $h(n)$ is the input, $w(n)$ is the impulse response (HDR), $v(n)$ is the disturbance, and $s(n)$ is the BOLD response.

The input $h(n)$ can be modeled using a boxcar function for block design. For an event-related design, the input can be modeled using a series of impulses of unit amplitudes at instances, where the stimuli are present [7]. $v(n)$ consists of slow-varying drift and white Gaussian noise. $w(n)$ is usually modeled as the difference between two gamma functions [22]

$$w(n) = \left(\frac{n}{d_1}\right)^{a_1} e^{(-(n-d_1)/b_1)} - c\left(\frac{n}{d_2}\right)^{a_2} e^{(-(n-d_2)/b_2)}. \tag{4}$$

The common choices of these parameters are $a_1 = 6, a_2 = 12, b_1 = b_2 = 0.9$ s, and $c = 0.35$. Observations from fMRI experiments have shown that HDRs vary among different brain regions and subjects [23], [24]. It is also reported that the HDRs may also vary from trial to trial [25], [26]. Therefore, in this paper, the HDR in each individual voxel of the brain is estimated using an adaptive filter.

### A. Adaptive Estimation

Adaptive filters are used to model the HDR. Given *a priori* knowledge of the input paradigm and fMRI signal, the HDR can be estimated from the filter coefficients of the adaptive filter shown in Fig. 1.

Here, $\mathbf{h}(n) = [h(n), h(n-1), h(n-2), \ldots, h(n-N+1)]^T$ is a known input stimulus vector, with $N$ being the filter length. $\mathbf{w}(n) = [w_1, w_2, w_3, \ldots, w_N]^T$ is the filter coefficient vector.

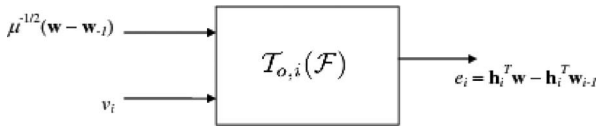


Fig. 2. Transfer operator from disturbances to output prediction error.

$d(n)$ is the measured fMRI signal [contaminated with disturbance $v(n)$], and $\hat{s}(n)$ is the estimate of the BOLD signal $s(n)$. Being the impulse response of the system, $\mathbf{w}(n)$ approximates the HDR function once the algorithm converges.

In this paper, we shall present four $H^\infty$ problem formulations and solutions. The estimation strategy is always to reduce the $H^\infty$ norm (i.e, $\|\mathcal{T}_{o,i}(\mathcal{F})\|_\infty^2$), which captures the worst case behavior of the system and can be regarded as the maximum energy gain from disturbances to prediction errors (see Fig. 2). Each problem has different forms of disturbances and prediction errors resulting in different transfer functions [1].

*1) Output Prediction Problem:* The problem here is to find an $H^\infty$ optimal estimation strategy $\mathcal{F}(\cdot)$, such that $\|\mathcal{T}_{o,i}(\mathcal{F})\|_\infty$ is minimized and obtain

$$\gamma_o^2 = \inf_{\mathcal{F}} \|\mathcal{T}_{o,i}(\mathcal{F})\|_\infty^2 \tag{5}$$

$$= \inf_{\mathcal{F}} \sup_{\mathbf{w}, v \in h_2} \frac{\sum_{j=0}^{i} \mid e_j \mid^2}{\mu^{-1} \mid \mathbf{w} - \mathbf{w}_{-1} \mid^2 + \sum_{j=0}^{i} \mid v_j \mid^2}. \tag{6}$$

In other words, we are minimizing the $H^\infty$ norm of the transfer operator $\mathcal{T}_{o,i}(\mathcal{F})$ that maps the unknown disturbances $\{\mu^{-1/2}(\mathbf{w} - \mathbf{w}_{-1}), \{v_j\}_{j=0}^i\}$ to the prediction errors $\{e_j\}_{j=0}^i$ (see Fig. 2). Here, $\mathbf{w}_{-1}$ is the initial estimate of the weight vector $\mathbf{w}$, and $\mu$ is a positive constant reflecting the *a priori* knowledge on how close $\mathbf{w}$ is to $\mathbf{w}_{-1}$. We denote the estimate of the weight vector using all the information available up till time $i$ by $\mathbf{w}_i$.

Solution to the output prediction problem is the well-known LMSs algorithm [27]. Since the LMS algorithm does not take into account possible time variations in the state vector, there is a need for problem formulations, which deal with such time variations. As the nature of time variations in HDR is unknown, we consider the following three problem formulations.

*2) Exponential Weights Problem:* A forgetting factor $0 < \lambda < 1$ is introduced such that more recent data are given more weightage, thus allowing us to track the time variations of the underlying models. We are to find an $H^\infty$ optimal estimation strategy and obtain

$$\gamma_\lambda^2 = \inf_{\mathcal{F}} \|\mathcal{T}_{\lambda,i}(\mathcal{F})\|_\infty^2 \tag{7}$$

$$= \inf_{\mathcal{F}} \sup_{\mathbf{w}, v \in h_2} \frac{\sum_{j=0}^{i} \lambda^{-j} \mid e_j \mid^2}{\mu^{-1} \mid \mathbf{w} - \mathbf{w}_{-1} \mid^2 + \sum_{j=0}^{i} \lambda^{-j} \mid v_j \mid^2}. \tag{8}$$

Note that the prediction error and disturbance energies are now in different forms compared to the previous problem. The solution to this problem is named the EW algorithm and the exponential bound $\gamma_\lambda$ is calculated as follows:

$$\gamma_\lambda^2 \leq \sup_i \frac{\overline{h} + \underline{\sigma}(\mathbf{R}_{\lambda,i})}{\lambda^i/\mu + \underline{\sigma}(\mathbf{R}_{\lambda,i})} \tag{9}$$

where $\overline{h} = \sup_i \mathbf{h}_i^T\mathbf{h}_i$, $\mathbf{R}_{\lambda,i} = \lambda^{-i}\sum_{j=0}^{i-1}\lambda^{-j}\mathbf{h}_j\mathbf{h}_j^T$, and $\underline{\sigma}(\mathbf{R}_{\lambda,i})$ denotes the maximum singular value of $\mathbf{R}_{\lambda,i}$. The algorithm is as follows:

$$\mathbf{w}_i = \mathbf{w}_{i-1} + \frac{\mathbf{P}_i\mathbf{h}_i}{1+\mathbf{h}_i^T\mathbf{P}_i\mathbf{h}_i}(d_i - \mathbf{h}_i^T\mathbf{w}_{i-1}) \tag{10}$$

$$\mathbf{P}_{i+1}^{-1} = \lambda\mathbf{P}_i^{-1} + \lambda\mathbf{h}_i\mathbf{h}_i^T - \gamma_\lambda^{-2}\mathbf{h}_{i+1}\mathbf{h}_{i+1}^T \tag{11}$$

initialized with $\mathbf{P}_0^{-1} = \mu^{-1}\mathbf{I} - \gamma_\lambda^{-2}\mathbf{h}_0\mathbf{h}_0^T$.

*3) FM Problem:* Also known as the sliding window problem, here one considers data from a finite window of length $L$. Therefore, as each new datum is observed, the least recent data are discarded. We are to find an $H^\infty$ optimal estimation strategy and obtain

$$\gamma_L^2 = \inf_{\mathcal{F}} \|\mathcal{T}_{L,i}(\mathcal{F})\|_\infty^2 \tag{12}$$

$$= \inf_{\mathcal{F}} \sup_{\mathbf{w},v\in h_2} \frac{\sum_{j=i-L+1}^{i} \mid e_j \mid^2}{\mu^{-1} \mid \mathbf{w}-\mathbf{w}_{-1} \mid^2 + \sum_{j=i-L+1}^{i} \mid v_j \mid^2}. \tag{13}$$

The FM algorithm allows us to cope with time variations in the underlying model as follows:

$$\gamma_L^2 \le \sup_i \frac{\overline{h} + \underline{\sigma}(\mathbf{R}_i^L)}{\mu^{-1} + \underline{\sigma}(\mathbf{R}_i^L)} \tag{14}$$

where $\mathbf{R}_i^L$ is $\sum_{j=i-L+1}^{i}\mathbf{h}_j\mathbf{h}_j^T$, and $\underline{\sigma}(\mathbf{R}_i^L)$ denotes the maximum singular value of $\mathbf{R}_i^L$. The update rule is as follows:

$$\mathbf{w}_{i-1}^d = \mathbf{w}_{i-1} + \frac{\mathbf{P}_i^d\mathbf{h}_{i-L}}{-1+\mathbf{h}_{i-L}^T\mathbf{P}_i^d\mathbf{h}_{i-L}}(d_{i-L} - \mathbf{h}_{i-L}^T\mathbf{w}_{i-1}) \tag{15}$$

$$(\mathbf{P}_i^d)^{-1} = \mathbf{P}_i^{-1} - (1-\gamma_L^{-2})\mathbf{h}_{i-L}\mathbf{h}_{i-L}^T \tag{16}$$

$$\mathbf{w}_i = \mathbf{w}_{i-1}^d + \frac{\mathbf{P}_i\mathbf{h}_i}{1+\mathbf{h}_i^T\mathbf{P}_i\mathbf{h}_i}(d_i - \mathbf{h}_i^T\mathbf{w}_{i-1}^d) \tag{17}$$

$$\mathbf{P}_{i+1}^{-1} = (\mathbf{P}_i^d)^{-1} - (1-\gamma_L^{-2})\mathbf{h}_{i+1}\mathbf{h}_{i+1}^T \tag{18}$$

initialized with $\mathbf{P}_0 = \mathbf{P}_0^d = \mu\mathbf{I}$.

*4) Time Variation Problem:* This problem deals with a TV filter model, instead of considering the underlying time variations of a time-invariant filter. The filter is of the form $d_i = \mathbf{h}_i^T\mathbf{x}_i + v_i$, where the state vector $\mathbf{x}_i$ is time-varying. Because of this, there is an additional disturbance term $\delta\mathbf{x}_i = \mathbf{x}_{i+1} - \mathbf{x}_i$, which is included in the problem

$$\gamma_g^2 = \inf_{\mathcal{F}} \|\mathcal{T}_{g,i}(\mathcal{F})\|_\infty^2 \tag{19}$$

$$= \inf_{\mathcal{F}} \sup_{\mathbf{x}_0,v,\delta\mathbf{x}\in h_2} \frac{\|e\|_2^2}{\mu^{-1} \mid \mathbf{x}_0 - \hat{\mathbf{x}}_0 \mid^2 + \|v\|_2^2 + q^{-1}\|\delta\mathbf{x}\|_2^2} \tag{20}$$

where $\|e\|_2^2 = \sum_{j=0}^{i} \mid e_j \mid^2$ and $\|\delta\mathbf{x}\|_2^2 = \sum_{j=0}^{i} \mid \delta\mathbf{x} \mid^2$. $q$ is a positive constant that reflects *a priori* knowledge on how fast the state vector varies with time. The solution to this problem is named as the TV algorithm

$$\gamma_g^2 \le 1 + q\bar{h}. \tag{21}$$

$$\mathbf{x}_{i+1} = \mathbf{x}_i + \frac{\mathbf{P}_i\mathbf{h}_i}{1+\mathbf{h}_i^T\mathbf{P}_i\mathbf{h}_i}(d_i - \mathbf{h}_i^T\hat{\mathbf{x}}_i) \tag{22}$$

$$\mathbf{P}_i^{-1} = \tilde{\mathbf{P}}_i^{-1} - \gamma_g^{-2}\mathbf{h}_i\mathbf{h}_i^T \tag{23}$$

$$\tilde{\mathbf{P}}_{i+1} = [\tilde{\mathbf{P}}_i^{-1} + (1-\gamma_g^{-2})\mathbf{h}_i\mathbf{h}_i^T]^{-1} + q\mathbf{I} \tag{24}$$

initialized with $\tilde{\mathbf{P}}_0 = \mu\mathbf{I}$.

*5) Recursive Least Square (RLS) Algorithm:* Since the RLS algorithm is not an $H^\infty$ algorithm, we will compare our analysis results against it. The RLS algorithm is presented here as follows:

$$\mathbf{g}_{i+1} = \frac{\mathbf{P}_i\mathbf{h}_i}{1+\mathbf{h}_i^T\mathbf{P}_i\mathbf{h}_i} \tag{25}$$

$$\mathbf{P}_{i+1} = \mathbf{P}_i - \mathbf{g}_{i+1}\mathbf{h}_i^T\mathbf{P}_i \tag{26}$$

$$\mathbf{w}_{i+1} = \mathbf{w}_i + \mathbf{g}_{i+1}(d_i - \mathbf{h}_i^T\mathbf{w}_i) \tag{27}$$

initialized with $\mathbf{P}_0 = \mu\mathbf{I}$.

The parameters mentioned hereafter will be consistent with the parameters in this section. Performances of the three $H^\infty$ algorithms (FM, EW, and TV) in HDR estimation and detection are investigated on both time-invariant and TV-HDRs.

## III. Results and Discussion

Preliminary investigations were conducted using time-invariant HDRs, before performing more detailed investigations using TV-HDRs. For both cases, the three $H^\infty$ algorithms were first run on simulated data to assess their performances in estimating the HDR, and estimation results were compared against that of the LMS and RLS algorithms. The activation detection abilities of the three algorithms were also investigated and compared against that of the conventional $t$-test method, as well as the LMS and RLS algorithms. The efficacy of these algorithms was then verified using real data. Results obtained by assuming a TV-HDR were compared against those obtained by a time-invariant HDR assumption.

### A. Simulated Data

*1) HDR Estimation: Time-invariant HDR:* Fig. 3 shows the simulated inputs (in red) and BOLD responses for each design. Fig. 4 shows 400 samples of the simulated fMRI signals for both block (SNR $\approx$ 5 dB) and event-related (SNR $\approx -5$ dB) designs consisting of the BOLD signal, slow-varying drift, and white Gaussian noise.

The simulated fMRI signals were investigated using the proposed $H^\infty$ filters, as well as the LMS and RLS algorithms. In determining the parameter values, a range of values were tested for each parameter, and the value for which the algorithm showed the best performance was used. Parameters used for this simulation are $\mu = 0.001, \lambda = 0.99999, q = 10^{-8}$, and $L = 6000$. In Fig. 5, the estimated HDRs are shown along with the actual HDR for both designs.

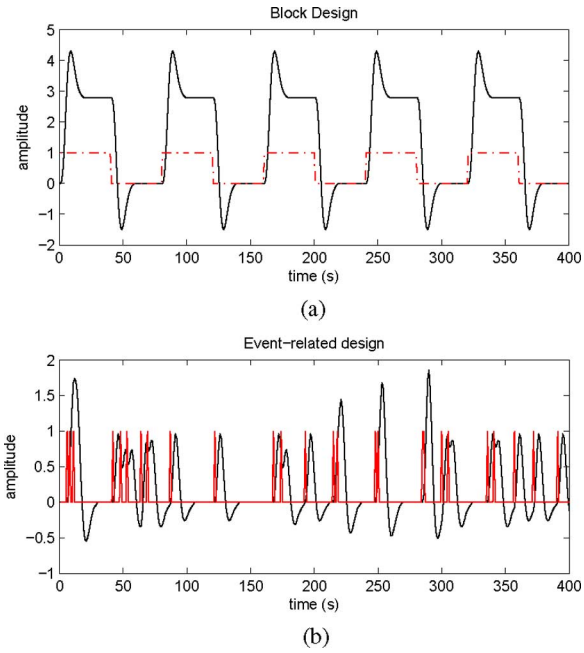


Fig. 3. Simulated input and BOLD signals. (a) Block design. (b) Event-related design.

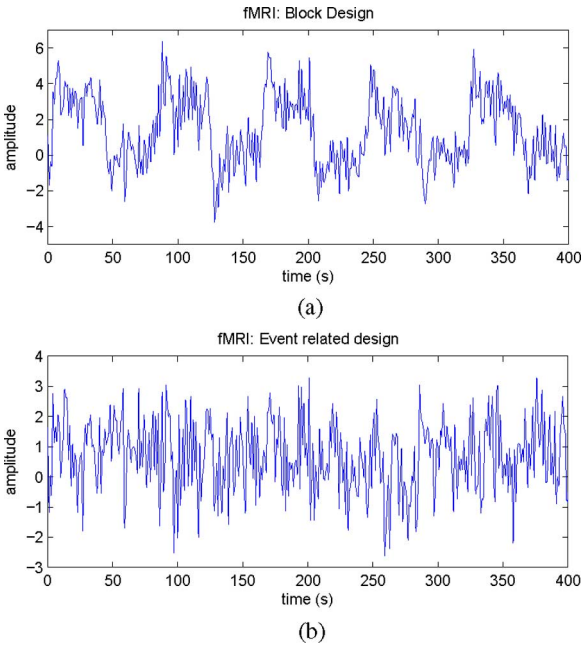


Fig. 4. Simulated fMRI signals. (a) Block design. (b) Event-related design.

In evaluating the filter performances, the normalized MSE (NMSE), defined in (29), is computed and shown in Table I

$$\text{NMSE} = \frac{\| \hat{\mathbf{w}} - \mathbf{w} \|^2}{\| \mathbf{w} \|^2} \tag{29}$$

where $\hat{\mathbf{w}}$ and $\mathbf{w}$ are the estimated and true HDR vectors, respectively.

From Fig. 5 and the NMSE values in Table I, it is clear that the filters are capable of accurately estimating the HDR. Furthermore, results from the LMS and RLS algorithms are

TABLE I
NMSEs IN HDR (TIME-INVARIANT) ESTIMATION

| | EW | TV | FM | LMS | RLS |
|---|---|---|---|---|---|
| Event-Related | 0.0068 | 0.0045 | 0.0053 | 0.0042 | 0.0080 |
| Block Design | 0.0082 | 0.0056 | 0.0061 | 0.0056 | 0.0088 |

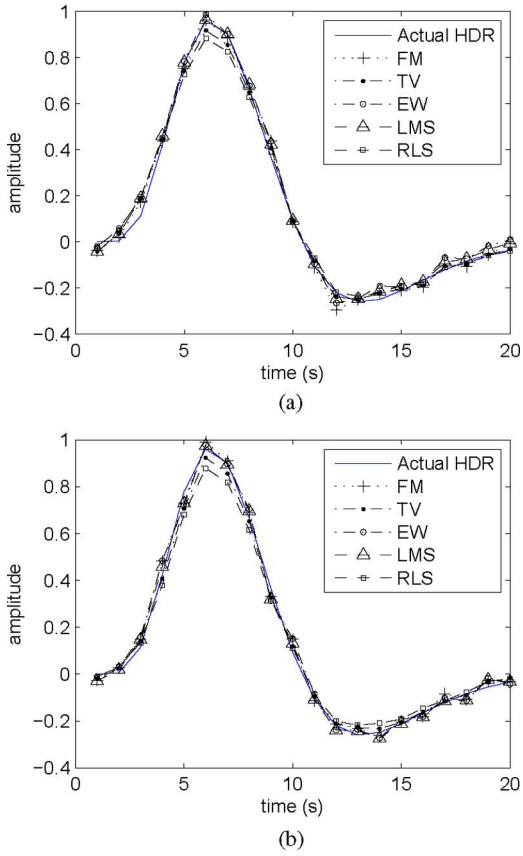


Fig. 5. HDR estimates. (a) Block design. (b) Event-related design.

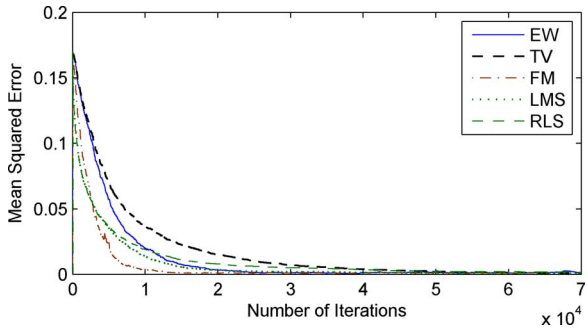


Fig. 6. Learning curves of the algorithms.

similar to that of the EW, FM, and TV algorithms. This shows that HDR estimation can be done by LMS when the HDR is not varying with time due to its simplicity. Also, HDR estimations are more accurate using the event-related design than the block design, which is in line with the fact that the event-related and block designs are used for HDR estimations and detections, respectively [8].

Fig. 6 shows the learning curves for the proposed algorithms. It can be seen from the graph that the FM algorithm converges

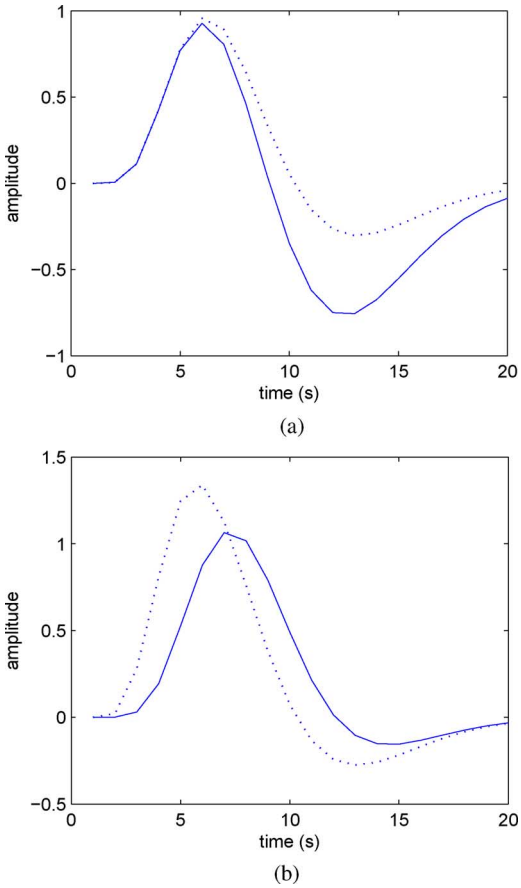


Fig. 7. HDRs 500 s apart. (a) Variation in undershoot. (b) Variation in delay.

the fastest (about 10 000 iterations). The TV and RLS algorithms converge the slowest (about 50 000 iterations).

*2) HDR Estimation: TV-HDR:* Here, we consider an event-related design. To simulate the variation of HDR, one of its parameters in the gamma function is changed based on a drift signal. This ensures that the general shape of the HDR remains unchanged. Since the variation of HDRs in real fMRI data is not well understood, we consider changes in both the HDR delay and undershoot (see Fig. 7).

To show the robustness of $H^\infty$ methods against different types of disturbances, we consider five types of noises (SNR ranging from $-10$ to 3 dB): *white noise* (type I), *white noise and drift* (type II), *drift* (type III), *bandpass filtered noise* (type IV), and *highpass filtered noise* (type V).

Parameters used for the simulations are $\mu = 0.015, \lambda = 0.999, q = 2 \times 10^{-5}$, and $L = 20$. The mean estimation errors in the state vector [defined in (30)] are computed for all algorithms in each run consisting of 1100 samples, and averaged over 500 independent runs. Results are tabulated in Tables II and III for HDR varying in undershoot and delay, respectively,

$$\text{Mean estimation error} = \frac{1}{N_t} \sum_{i=0}^{N_t} \| \hat{\mathbf{w}}_i - \mathbf{w}_i \|^2 \qquad (30)$$

where $N_t$ is the total number of samples. $\hat{\mathbf{w}}_i$ and $\mathbf{w}_i$ are the estimated and true HDR vectors, respectively, at time $i$.

TABLE II
MEAN ESTIMATION ERRORS (VARIATIONS IN UNDERSHOOT)

| Noise type | EW | FM | TV | LMS | RLS |
|---|---|---|---|---|---|
| I | 0.0920 | 0.0916 | 0.0914 | 0.0963 | 0.1065 |
| II | 0.0935 | 0.0924 | 0.0935 | 0.0977 | 0.1055 |
| III | 0.0979 | 0.0793 | 0.0985 | 0.1080 | 0.1180 |
| IV | 0.0895 | 0.0831 | 0.0891 | 0.0897 | 0.1096 |
| V | 0.0869 | 0.0819 | 0.0899 | 0.0976 | 0.1076 |

TABLE III
MEAN ESTIMATION ERRORS (HDRs VARYING IN DELAY)

| Noise type | EW | FM | TV | LMS | RLS |
|---|---|---|---|---|---|
| I | 0.1016 | 0.0886 | 0.1021 | 0.1126 | 0.1285 |
| II | 0.1085 | 0.0911 | 0.1092 | 0.1229 | 0.1419 |
| III | 0.0943 | 0.0762 | 0.0959 | 0.1120 | 0.1309 |
| IV | 0.0979 | 0.0789 | 0.0990 | 0.1137 | 0.1326 |
| V | 0.0931 | 0.0781 | 0.0945 | 0.1098 | 0.1286 |

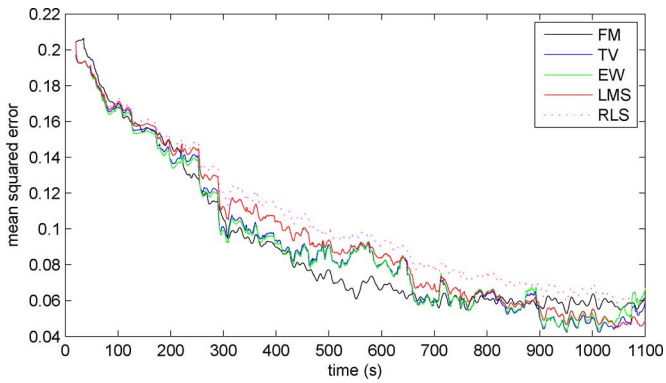


Fig. 8. Learning curves of algorithms under type II noise (HDR varying in undershoot).

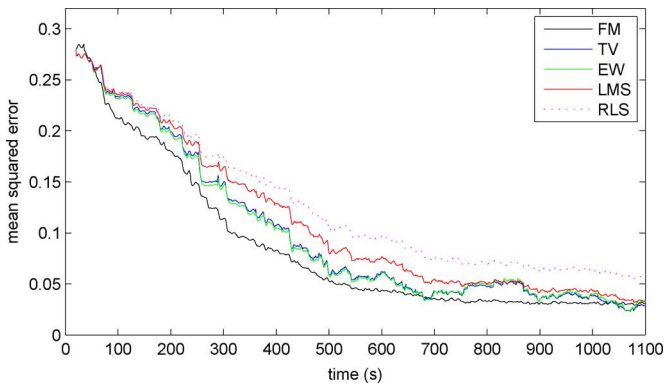


Fig. 9. Learning curves of algorithms under type I noise (HDR varying in delay).

Results in Tables II and III clearly show that the EW, FM, and TV algorithms, which cope with time variations, outperform the LMS and RLS algorithms for all types of disturbances and HDR variations. In addition, LMS performs better than RLS, since the former is an $H^\infty$ algorithm and is therefore more robust and less sensitive to state-vector variations [27].

Figs. 8 and 9 show the learning curves of the algorithms under different disturbances and HDR variations. Similar graphs are

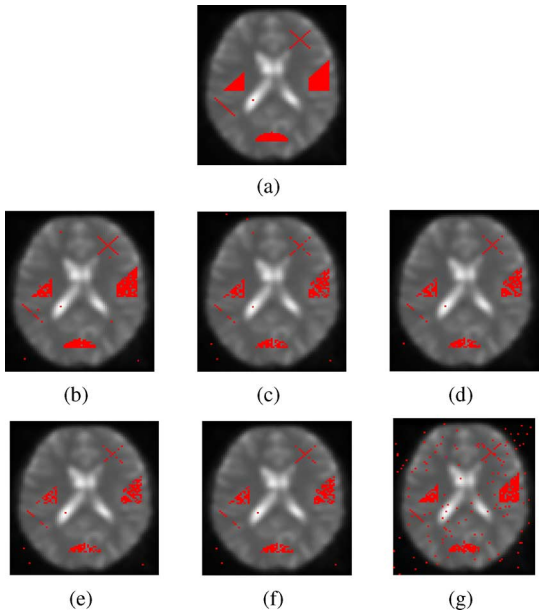


Fig. 10. Detection results of the simulated fMRI data. (a) Simulated brain activations. (b) FM algorithm ($\rho > 0.4$). (c) EW algorithm ($\rho > 0.4$). (d) TV algorithm ($\rho > 0.45$). (e) LMS algorithm ($\rho > 0.4$). (f) RLS algorithm ($\rho > 0.4$). (g) Conventional $t$-test ($p < 0.001$).

obtained for other types of noise (figures not shown). From these graphs, it is seen that the FM algorithm has the fastest convergence rate. Furthermore, learning curves corresponding to the LMS and RLS algorithms are above that of the FM, TV, and EW algorithms most of the time. This could be because LMS and RLS are poorer in coping with time variations.

*3) Detection of Brain Activations: Time-Invariant HDR:* The detection abilities using the FM, EW, and TV algorithms are compared against that of the LMS and RLS algorithms, as well as the conventional $t$-test method, which the average signal during the task to the average signal during the rest period [28].

In coming up with the simulations, a slice from a set of real fMRI data was used as the background image. Simulated BOLD signals generated by different TV-HDRs (parameter $c$ varies between $-1$ and 1 for each voxel) were added to certain voxels in the brain. Disturbance signals consisting of Gaussian white noises and drifts of varying powers were added to all voxels, forming a 3-D fMRI time series having various SNRs. Eighty samples were used in this simulation. For the FM algorithm, $\mu = 0.01$ and $L = 20$. For the TV algorithm, $\mu = 0.002$ and $q = 10^{-8}$, and for EW algorithm, $\mu = 0.001$ and $\lambda = 0.99999$. For both the LMS and RLS algorithms, $\mu = 0.001$.

Each algorithm was run over all voxels in the brain scan. The estimated HDR in each voxel was then convolved with the input stimulus function to obtain the reconstructed BOLD signal. The correlation coefficient between the reconstructed BOLD signal and the simulated fMRI signal was then computed for each voxel. Statistical parametric map (SPM) was then performed by comparing the correlation coefficients against a threshold value. A voxel was considered active if the correlation coefficient exceeded the threshold, otherwise it was deemed inactive. Fig. 10(b)–(d) shows the detections using the proposed $H^\infty$ algorithms. For the conventional $t$-test, if the $t$-statistic in a particular voxel was greater than the voxel's threshold value, then that voxel was considered active [see Fig. 10(g)]. Correlation values were chosen such that the detections showed the best mapping result. These threshold values (around 0.3 to 0.45) were used for reference in deciding the threshold values for real data, which shall be examined later on. From these results, we can see that the $H^\infty$ algorithms clearly outperform the conventional $t$-test method. The $t$-test method results in many false detections, while the proposed algorithms can accurately detect the activated regions and minimize the number of false detections.

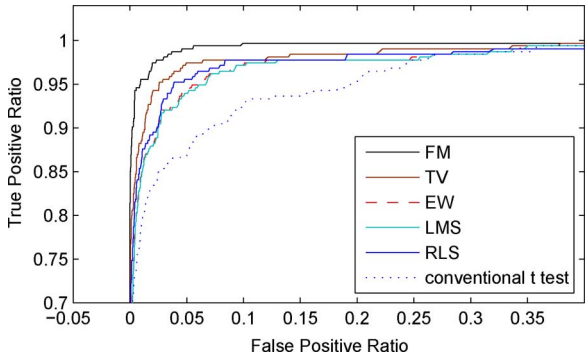


Fig. 11. ROC curves for the detection methods.

The performances of the algorithms were further investigated by studying the receiver–operator characteristic (ROC) curve (see Fig. 11) [29]. The ROC curve is a plot of true-positive ratio (proportion of correctly detected voxels to all actual activated voxels) against false-positive ratio (proportion of voxels that were incorrectly deemed active to all actual inactivated voxels). A method that detects the most real activations while minimizing the number of false detections is the most desirable. From Fig. 11, it is clear that all three $H^\infty$ algorithms outperform the conventional method, with the FM algorithm showing the best detection ability. We also see that the LMS and RLS algorithms have similar detection abilities compared to the EW, FM, and TV algorithms.

*4) Detection of Brain Activations—TV-HDR:* The ability of the algorithms in detecting activations was further investigated using TV-HDRs. Investigations were carried out in a similar manner for the time-invariant case, expect that all the HDR estimates were used in reconstructing the BOLD signal. This is unlike the time-invariant case, in which only the final HDR estimate is used in reconstructing the BOLD signal. Three hundred samples were used in this simulation. Parameters used are $\mu = 0.015, \lambda = 0.999, q = 7 \times 10^{-5}$, and $L = 10$.

From Fig. 12, it is obvious that the proposed $H^\infty$ algorithms outperform the LMS and RLS algorithms in brain activation detections with fewer false detections and more true detections. The performances of the algorithms were further investigated by studying the ROC curve (see Fig. 13) [29]. From Fig. 13, it is clear that the EW, FM, and TV algorithms outperform the LMS and RLS algorithms, with RLS having the poorest detection ability due to its poor robustness.

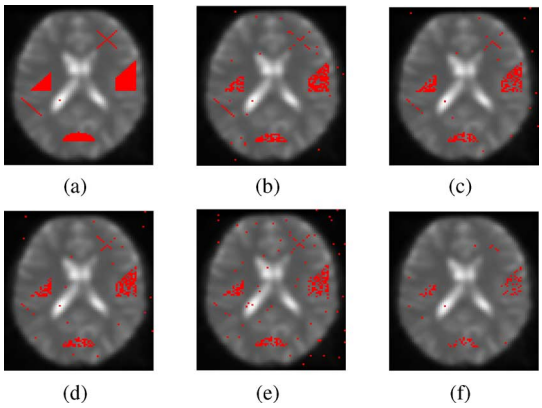


Fig. 12. Detection results of the simulated fMRI data. (a) Simulated brain activations. (b) FM algorithm ($\rho > 0.34$). (c) EW algorithm ($\rho > 0.38$). (d) TV algorithm ($\rho > 0.45$). (e) LMS algorithm ($\rho > 0.38$). (f) RLS algorithm ($\rho > 0.25$).

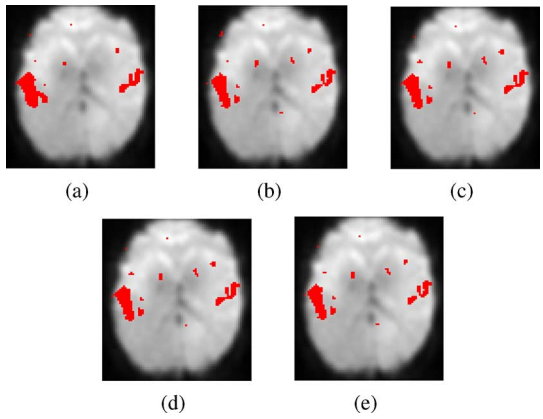


Fig. 14. Detection of auditory cortex (assuming time-invariant HDR). (a) FM algorithm ($\rho > 0.3$). (b) EW algorithm ($\rho > 0.3$). (c) TV algorithm ($\rho > 0.3$). (d) LMS algorithm ($\rho > 0.3$). (e) RLS algorithm ($\rho > 0.3$).

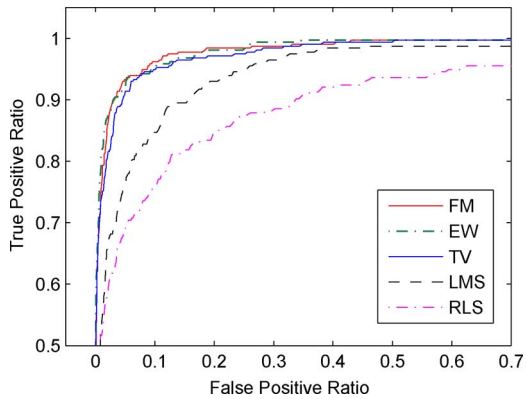


Fig. 13. ROC curves for the detection methods.

### B. Real fMRI Data

The ability of the $H^\infty$ algorithms to perform accurate activation detections was also verified on two sets of real fMRI data: DATA-EVENT (event-related design) and DATA-BLOCK (block design). Both data sets were obtained from the National fMRI Data Center (http://www.fmridc.org). Detections that assume a time-invariant HDR are compared against the detection results obtained by assuming a TV-HDR.

*1) DATA-EVENT:* This data were from an event-related experiment (with the accession number 2-2000-11127) [30]. This experiment investigated the activity in the human calcarine sulcus (which contains the primary visual cortex) during single instances of mental imagery. Each experiment began with a 2-s auditory presentation of an animal's name. After 14 s, a second auditory presentation of a possible characteristic of the animal was made. Following this, the subjects evaluated the characteristic of the animal. Several such visual–mental processes were made. Each experiment contained 308 data points and each fMRI scan was 2 s apart (repetition time TR $= 2$ s). From the description of the experiment, we learn that the subjects were given auditory stimuli. Thus, the auditory cortex and the Wernicke's area (next to the auditory cortex and used for speech processing) should be activated during instances when the auditory stimulus was present. In this paper, we investigate the activation of these two regions.

The input stimulus function was inferred from the experiment description. The data were preprocessed (for realignment, normalization, and spatial smoothing) using the SPM software [31]. The $H^\infty$ algorithms were then used to analyze the data and perform activation detections. Since the data had a sampling period of 2 s, the length ($N$) of the filter coefficient in the adaptive filter was chosen to be 10, such that the estimated HDR lasts for 18 s.

Detections were first performed on the data by assuming a time-invariant HDR (see Fig. 14). For the FM algorithm, $\mu = 0.01$ and $L = 20$. For the TV algorithm, $\mu = 0.002$ and $q = 10^{-8}$, and for EW algorithm, $\mu = 0.001$ and $\lambda = 0.99999$. For both LMS and RLS algorithms, $\mu = 0.001$.

Detections on the same set of real data were further investigated by assuming a TV-HDR. The analysis procedure was similar to the time-invariant case, except that the BOLD signal was reconstructed differently. After the algorithms were run on the dataset containing 308 samples, the first 108 HDR estimates were discarded and the 200 most recent estimates were used in reconstructing the BOLD signal. This allows better signal reconstruction, since the first 108 HDR estimates were not well-learnt. Parameters used for this experiment are $\mu = 0.1$, $L = 10$, $q = 3 \times 10^{-5}$, and $\lambda = 0.999$. The detection results are shown in Fig. 15. As seen, performances among the algorithms are approximately the same, with the proposed $H^\infty$ algorithms having slightly better detections than the LMS and RLS algorithms, since they detect a slightly bigger region of activation, which is closer to the expected size.

Detections show slightly different activated areas for different assumptions made on the HDR. Comparing this set of results to those obtained using the time-invariant assumption, there is a slight displacement in the active area for the right side of the brain. However, both regions correspond to a part of the auditory cortex and Wernicke's area. In the absence of the ground truth, we cannot determine which assumption on HDR variation leads to a better detection in this case.

*2) DATA-BLOCK:* The second set of data (DATA-BLOCK, with accession number 2-2000-111JJ) was designed for

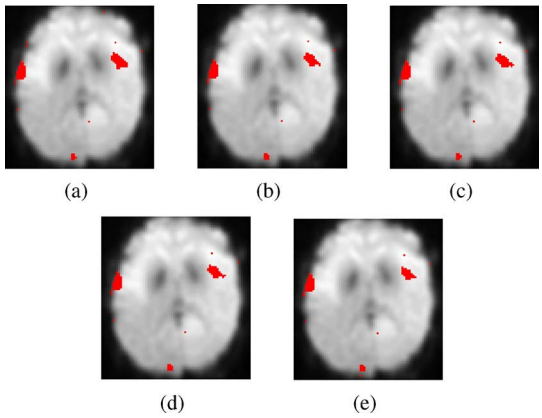


Fig. 15. Detection of auditory cortex (assuming TV-HDR). (a) FM algorithm ($\rho > 0.3$). (b) EW algorithm ($\rho > 0.3$). (c) TV algorithm ($\rho > 0.3$). (d) LMS algorithm ($\rho > 0.3$). (e) RLS algorithm ($\rho > 0.3$).

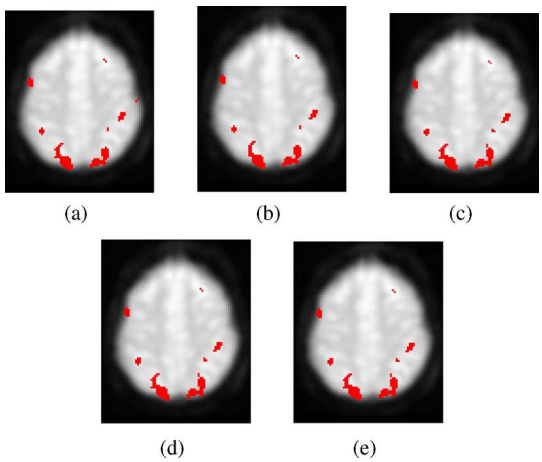


Fig. 16. Detection of visual cortex (assuming time-invariant HDR). (a) FM algorithm ($\rho > 0.45$). (b) EW algorithm ($\rho > 0.45$). (c) TV algorithm ($\rho > 0.45$). (d) LMS algorithm ($\rho > 0.45$). (e) RLS algorithm ($\rho > 0.45$).

visuospatial processing task—judgement of line orientation [32]. This set of data contains 100 fMRI scans, each obtained 3 s apart (TR=3 s). The experiment lasted for 5 min. During the baseline condition, the subjects were asked to determine if two stimulus lines on the screen were at the same level. During the activation condition, nine radial lines arranged in a semicircle were shown in the bottom half of the screen. The subjects had to decide if the two stimulus lines shown in the top half of the screen were oriented in the same way as the two highlighted lines in the bottom half. Thus, this experiment activates the visual cortex of the brain.

Again, investigations were first carried out using the time-invariant assumption (see Fig. 16). Filter length ($N$) was chosen to be 7. For the FM algorithm, $\mu = 0.01$ and $L = 20$. For the TV algorithm, $\mu = 0.002$ and $q = 10^{-8}$, and for EW algorithm, $\mu = 0.001$ and $\lambda = 0.99999$. For both LMS and RLS algorithms, $\mu = 0.001$.

Similar investigations were carried out by assuming a TV-HDR. However, since all the estimated HDRs have to be used to reconstruct the BOLD signal and there are only 100

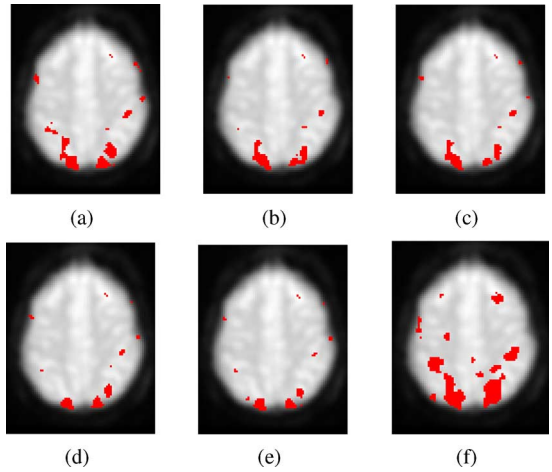


Fig. 17. Detection of visual cortex (assuming TV HDR). (a) FM algorithm ($\rho > 0.33$). (b) EW algorithm ($\rho > 0.4$). (c) TV algorithm ($\rho > 0.39$). (d) LMS algorithm ($\rho > 0.33$). (e) RLS algorithm ($\rho > 0.3$). (f) Conventional $t$-test ($p < 0.001$).

samples available, the HDR estimates might not be well learned. To overcome this problem, the dataset were first run on LMS algorithm and the final HDR estimate is then used to initialize the filters. For the FM algorithm, $\mu = 0.1$ and $L = 8$. For the TV algorithm, $\mu = 0.22$ and $q = 3 \times 10^{-5}$. For the EW algorithm, $\mu = 0.35$ and $\lambda = 0.999$, and for the LMS and RLS algorithms, $\mu = 0.2$. Detection was also performed using the conventional $t$-test method at 99.9% significance level. From Fig. 17(f), it is clear that there are many false detections, proving that $H^\infty$ algorithms outperform the conventional $t$-test method. From the detection results in Fig. 17, we can see that the visual cortex is correctly detected by all the algorithms, with the LMS and RLS algorithms having poorer detection results, since their detected regions are smaller than what is expected. For good detections, the entire set of 100 HDRs have to be rather good estimates, since all of them would be used in BOLD signal reconstruction. With LMS and RLS algorithms having slower convergence rates (seen in the convergence curves previously), poor estimates of HDRs would be obtained, thus resulting in poorer detections. Similarly, since the EW algorithm is able to work with the largest learning parameter ($\mu = 0.35$), its detection result is the best due to its fastest rate of convergence.

Comparing the two sets of detection results, we notice that detection by the EW algorithm under time-varying assumption produces the best detection. However, we also see that there is not much difference between the two sets of detections, leading us to conclude that there is not much time variations in the HDR for this dataset. In such cases, it is more convenient to perform detections by assuming time invariance since the LMS algorithm, which can then be used, is much simpler. However, due to their better abilities in coping with time variations in the HDR (as shown in simulated data), the EW, TV, and FM algorithms can be used for datasets that do not show good detections under the time-invariance assumption.

For many years, researchers have been exploring the mystery of the most complex and enigmatic organ in the human body—the brain. With the developments in cognitive neuroscience,

many mysteries are gradually becoming clear to the scientific community. During the past decade, fMRI has been emerged as a powerful noninvasive neuroimaging technique for studying the brain's functions based on the HDR related to neural activity in the brain. It is becoming the diagnostic method of choice for learning how a normal, diseased, or injured brain is working, as well as for assessing the potential risks of surgery or other invasive treatments of the brain.

The intrinsic complexity of the brain functions as well as the data acquisition procedure makes the fMRI data analysis a difficult task. Estimation of the HDR is an important step in the processing and analysis of fMRI data. The time variations of the HDRs as well as the lack of knowledge of the statistical distribution of the disturbances make its estimation a challenging problem. In such situations, the use of $H^\infty$ approach in parameter estimation is proved to be optimal [1], [2]. Accordingly, in this paper, we proposed three robust signal processing algorithms based on the $H^\infty$ approach to the estimation of the HDRs in fMRI data analysis. The extensive simulation studies show the efficacy of these algorithms compared to the LMS and RLS algorithms.

### C. Potential Limitations of Proposed Algorithms

Parameter choices (such as the forgetting factor $\lambda$ in EW algorithm, window length $L$ in FM algorithm, and the parameter $q$ in TV algorithm) greatly affect the performance of the algorithms. However, currently there is no optimal way of determining these parameters and are determined empirically in carrying out the numerical simulations in our studies.

Another limitation is the computational complexity of the proposed algorithms. They are slightly computationally more intensive than the LMS algorithm. Therefore, these algorithms should not be used for time-invariant problems or those which involve little time variations. In such situations, the LMS algorithm should be used instead.

## IV. Conclusion

HDR estimation and detection are vital in fMRI data analysis. In this paper, three $H^\infty$ based adaptive filters, namely the FM, EW, and TV, were proposed to estimate the TV-HDRs. Through extensive numerical simulations (on simulated as well as real fMRI data), it is shown that these algorithms are capable of estimating the HDR accurately and outperform the conventional $t$-test method in detecting the activated regions of the brain. Investigations using phantom data containing TV-HDRs also show that the proposed $H^\infty$ algorithms perform better than the LMS and RLS algorithms, which do not cope with time variations. Thus, the proposed methods would be useful in cases, where fMRI data contains much time variations in the HDR.

## References


[1] B. Hassibi and T. Kailath, "$H^\infty$ adaptive filtering," in *Proc. ICASSP*, 1995, vol. 2, pp. 949–952.

[2] T. Ratnarajah and S. Puthusserypady, "An $H^\infty$ approach to adaptive minimization of EOG artefacts from EEG signals," in *Proc. 8th IEEE Workshop* DSP, 1998, pp. 1483–1487.

[3] K. Najarian and R. Splinter, *Biomedical Signal and Image Processing*. Boca Raton, FL: CRC, 2006.

[4] G. Nardulli and S. Stramaglia, *Modelling Biomedical Signals*. Singapore: World Scientific, 2002.

[5] G. E. Wnek and G. L. Bowlin, *Encyclopedia of Biomaterials and Biomedical Engineering*. London, U.K.: Informa Health Care, 2008.

[6] R. B. Buxton, *Introduction to Functional Magnetic Resonance Imaging: Principles and Techniques*. Cambridge, U.K.: Cambridge Univ. Press, 2002, ch. 6.

[7] P. Jezzard, P. Matthews, and S. Smith, *Functional MRI: An Introduction to Methods*. London, U.K.: Oxford Univ. Press, 2001.

[8] H. E. Luo and S. Puthusserypady, "Adaptive spatio-temporal modelling and estimation of the event-related fMRI responses," *Signal Process.*, vol. 87, no. 11, pp. 2810–2822, 2007.

[9] A. Dale and R. Buckner, "Selective averaging of rapidly presented individual trials using fMRI," *Hum. Brain Mapp.*, vol. 5, pp. 329–340, 1997.

[10] K. J. Friston, A. P. Holmes, J. B. Poline, P. J. Grasby, S. C. Williams, R. S. Frackowiak, and R. Turner, "Analysis of fMRI time-series revisited," *NeuroImage*, vol. 2, no. 1, pp. 45–53, 1995.

[11] K. J. Worsley and K. J. Friston, "Analysis of fMRI time-series revisited–again," *NeuroImage*, vol. 2, no. 3, pp. 173–235, 1995.

[12] V. P. Clark and J. V. Haxby, "fMRI study of face perception and memory using random stimulus sequences," *Neurophysiology*, vol. 79, no. 6, pp. 3257–3265, 1998.

[13] G. M. Boynton, S. A. Engel, G. H. Glover, and D. J. Heeger, "Linear systems analysis of functional magnetic resonance imaging in human V1," *Neuroscience*, vol. 16, no. 13, pp. 4207–4221, 1996.

[14] R. M. Birn, Z. S. Saad, and P. A. Bandettini, "Spatial heterogeneity of the nonlinear dynamics in the fMRI BOLD response," *NeuroImage*, vol. 14, pp. 817–826, 2001.

[15] K. J. Friston, A. Mechelli, R. Turner, and C. J. Price, "Nonlinear responses in fMRI: The balloon model, volterra kernels, and other hemodynamics," *NeuroImage*, vol. 12, pp. 466–477, 2000.

[16] R. Buxton, K. Uludag, D. J. Dubowitz, and T. T. Liu, "Modelling the hemodynamic response to brain activation," *NeuroImage*, vol. 23, pp. S220–S233, 2004.

[17] C. Goutte, F. Nielsen, and L. Hansen, "Modelling the haemodynamic response in fMRI with smooth FIR filters," *IEEE Trans. Med. Imag.*, vol. 19, no. 12, pp. 1188–1201, Dec. 2000.

[18] P. Ciuciu, J.-B. Poline, G. Marrelec, J. Idier, C. Pallier, and H. Benali, "Unsupervised robust non-parametric estimation of the hemodynamic response function for any fMRI experiment," *IEEE Trans. Med. Imag.*, vol. 22, no. 10, pp. 1235–1251, Oct. 2003.

[19] F. Å. Nielsen, L. K. Hansen, P. Toft, C. Goutte, N. Lange, S. C. Strother, N. Mørch, C. Svarer, R. Savoy, B. Rosen, E. Rostrup, and P. Born. (May 1997), "Comparison of two convolution models for fMRI time series," in *NeuroImage* [Online]. L. Friberg, A. Gjedde, S. Holm, N. A. Lassen, and M. Novak, Eds., vol. 5. San Diego, CA: Academic, May 1997, p. S473. Available: http://www2.imm.dtu.dk/pubdb/p.php?5215

[20] A. W. Toga and J. C. Mazziotta, *Brain Mapping: The Methods*. New York: Academic, 2002.

[21] B. Hassibi and T. Kailath, "Adaptive filtering with an $H^\infty$ criterion," in *Proc. 28th Asilomar Conf. Signals, Syst. Comput.*, 1994, pp. 1483–1487.

[22] K. Friston, P. Fletcher, O. Josephs, A. Holmes, M. Rugg, and R. Turner, "Event-related fMRI: Characterising differential responses," *NeuroImage*, vol. 7, pp. 30–40, 1998.

[23] B. Bonakdarpour, T. B. Parrish, and C. Thompson, "Hemodynamic response function in patients with stroke-induced aphasia: Implications for fMRI data analysis," *NeuroImage*, vol. 36, no. 2, pp. 322–331, 2007.

[24] D. A. Handwerker, J. M. Ollinger, and M. D. 'Esposito, "Variation of BOLD hemodynamic responses across subjects and brain regions and their effects on statistical analysis," *NeuroImage*, vol. 21, pp. 1639–1651, 2004.

[25] J. R. Duann, T. P. Jung, W. J. Kuo, T. C. Yeh, S. Makeig, J. C. Hsieh, and J. T. Sejnowski, "Single-trial variability in event-related BOLD signals," *NeuroImage*, vol. 15, no. 4, pp. 823–835, 2002.

[26] Y. Lu, T. Jiang, P. Lundberg, M. Borga, and H. Knutsson, "Single-trial variable model for event related fMRI data analysis," *IEEE Trans. Med. Imag.*, vol. 24, no. 2, pp. 236–245, Feb. 2005.

[27] B. Hassibi, A. H. Sayed, and T. Kailath, "$H^\infty$ optimality of the LMS algorithm," *IEEE Trans. Sig. Process.*, vol. 44, no. 2, pp. 267–280, Feb. 1996.

[28] G. E. Sarty, *Computing Brain Activity Maps from fMRI Time-Series Images*. 2nd ed. Cambridge, U.K.: Cambridge Univ. Press, 2006.

[29] R. Constable, P. Skudlarski, and J. Gore, "An ROC approach for evaluating functional brain MR imaging and postprocessing protocols," *Magn. Reson. Med.*, vol. 34, pp. 57–64, 1995.
[30] I. Klein, A. Paradis, J. Poline, S. Kosslyn, and D. Bihan, "Transient activity in the human calcarine cortex during visual-mental imagery: An event-related fMRI study," *Cogn. Neurosci.*, vol. 12, no. 2, pp. 15–23, 2000.
[31] J. Chumbley and H. Ouden, *SPM 99 course notes*, Wellcome Depart. Cogn. Neurol., Univ. College London, U.K., 2001, pp. 1–86.
[32] V. Ng, E. Bullmore, G. de Zubicaray, A. Cooper, J. Suckling, and S. Williams, "Identifying rate-limiting nodes in large-scale cortical networks for visuospatial processing: An illustration using fMRI," *J. Cogn. Neurosci.*, vol. 13, pp. 537–545, 2001.

**S. Puthusserypady** (M'00–SM'05) received the B.Tech degree in electrical engineering and the M.Tech degree in instrumentation and control systems engineering from the University of Calicut, Kozhikode, India, in 1986 and 1989, respectively, and the Ph.D. degree in electrical communication engineering from the Indian Institute of Science, Bengaluru, India, in 1995.

From 1993 to 1996, he was a Research Associate with the Department of Psychopharmacology, National Institute of Mental Health and Neurosciences, Bengaluru. From 1996 to 1998, he was a Postdoctoral Research Fellow with the Communications Research Laboratory, McMaster University, Hamilton, ON, Canada. In 1998, he was a Senior Systems Engineer with Raytheon Systems Canada Ltd., Waterloo, ON. During 2000 through 2009, he was an Assistant Professor with the Department of Electrical and Computer Engineering, National University of Singapore, Singapore. He is currently an Associate Professor with the Department of Electrical Engineering, Technical University of Denmark, Lyngby, Denmark. His research interests include biomedical signal processing, brain–computer interface, and home health care systems.

**Rui Jue** received the B.Eng degree in electrical engineering from the National University of Singapore (NUS), Singapore, in 2009.

From August 2008 to April 2009, she was a short-term Research Student with NUS, where she was engaged in studying $H^{\infty}$ adaptive filtering. She is currently a Research Engineer with DSO National Laboratories, Singapore. Her research interests include the areas of adaptive signal processing, biomedical signal processing, sensor networks, and array signal processing.

**T. Ratnarajah** (S'94–M'05–SM'05) received the B.Eng. (Hons.), M.Sc., and Ph.D. degrees.

Since 1993, he was with University of Ottawa, Ottawa, ON, Canada, Nortel Networks, Ottawa, McMaster University, Hamilton, ON, and Imperial College, London, U.K. He is currently a Principal Research Engineer with the Institute for Electronics, Communications, and Information Technologies, Queen's University Belfast, Belfast, UK. His research interests include random matrices theory, information theoretic aspects of multiple-input and multiple-output channels and ad hoc networks, wireless communications, signal processing for communication, statistical and array signal processing, biomedical signal processing, and quantum information theory. He has authored or coauthored more than 80 publications in these areas. He holds four U.S. Patents.

Dr. Ratnarajah is a member of American Mathematical Society and the Information Theory Society.